



# Exploring the use of graphene lubricant and TiO<sub>2</sub> nanolubricants in micro deep drawing of stainless steel SUS301

Di Pan<sup>1</sup> · Guangqing Zhang<sup>1</sup> · Fanghui Jia<sup>1</sup> · Hui Wu<sup>1</sup> · Yao Lu<sup>2</sup> · Tao Zhang<sup>1</sup> · Lianjie Li<sup>1</sup> · Fei Lin<sup>1</sup> · Ming Yang<sup>3</sup> · Zhengyi Jiang<sup>1</sup>

Received: 6 July 2023 / Accepted: 27 December 2023 / Published online: 25 January 2024  
© The Author(s) 2024

## Abstract

This study investigates the effects of different lubrication conditions on drawing force and microcup formation during micro deep drawing (MDD). Results show that graphene lubricant, in combination with TiO<sub>2</sub> nanolubricants, has the potential to reduce friction during MDD. The peak drawing force was reduced by 15.39% when both lubricants were used together, while the use of TiO<sub>2</sub> nanolubricant and 10.0 mg/ml graphene lubricant reduced it by 6.03% and 14.52%, respectively. The study also reveals that lubricants reduce wrinkling during the formation of microcups by minimising energy consumption during the primary formation. However, the combination of TiO<sub>2</sub> nanolubricant and graphene lubricant can cause inhomogeneous formation on the upper part of the blank, leading to more apparent wrinkling. Overall, the study highlights the potential of TiO<sub>2</sub> nanolubricant and graphene lubricant in reducing friction and improving microcup formation during MDD.

**Keywords** Micro deep drawing · TiO<sub>2</sub> nanolubricant · Graphene lubricant · Wrinkling minimisation

## 1 Introduction

In the last decade, the utilisation of micro deep drawing (MDD) has become crucial in the creation of micro-scale cup or box-shaped items, a popularity attributed to its affordability, high productivity, and ease of operation [1–3]. In an investigation on MDD, Luo et al. [4] identified critical role of friction, significantly impacting wear patterns and the final shape due to micro-scale surface and material variations. Fejkiel and Goleń [5] applied the finite element method to simulate friction in strip drawing tests. Their research suggests increased friction, driven by surface roughness and contact area, could boost required forces, potentially diminishing final product formability. Although using lubricants is a standard method for reducing friction,

their application at the micro scale presents challenges. Specifically, it may lead to premature lubricant film leakage, thereby failing to avert direct contact between the tool and the sample [6].

To avoid the leakage of the lubricant, using the nanolubricant has been a topic of much interest [7]. Alves et al. [8] formulated nanolubricants using small CuO nanoparticles (NPs). They suggested NP integration could amplify film thickness, securing adequate lubrication. Jason et al. [9] emphasised the potential of nanolubricants in reducing friction. They suggested that the introduction of NPs into the lubricant could transform sliding motion to rolling, further diminishing friction. Generally, the shape, dispersion, and size of the adding NPs are crucial to determine the performance of the lubricants [10, 11]. Research conducted by Trung et al. [12] and Esfe et al. [13] demonstrated the remarkable friction reduction capabilities of glycerol-based lubricants when infused with TiO<sub>2</sub> NPs. Efficient dispersion of TiO<sub>2</sub> NPs in glycerol resulted in decreased friction, leading to improved overall efficiency and product quality in manufacturing processes. Kumar et al. [14] utilised a variety of TiO<sub>2</sub> nanolubricant concentrations in a servo system lubricating oil and investigated the physicochemical and tribological properties using a sonication process. They found that the nanoparticles were unable to significantly

✉ Zhengyi Jiang  
jiang@uow.edu.au

<sup>1</sup> School of Mechanical, Materials, Mechatronic and Biomedical Engineering, Wollongong, NSW 2522, Australia

<sup>2</sup> Welding Engineering and Laser Processing Centre, Cranfield University, Bedfordshire MK43 0AL, UK

<sup>3</sup> Graduate School of System Design, Tokyo Metropolitan University, 6-6-Asahigaoka, Hino, Tokyo 191-0055, Japan

reduce friction at lower concentrations, and the performance of the lubricant was negatively impacted by the substantial agglomeration that occurred at higher TiO<sub>2</sub> concentrations.

To address the issues of insufficient lubricant film and agglomeration of nanolubricants, it may be worthwhile to explore the potential of solid lubricants as an alternative. Graphene, which is a two-dimensional substance made up of a solitary layer of carbon atoms structured in a pattern akin to a honeycomb, has been studied for its potential as a solid lubricant [15–17]. Lin et al. [18] highlighted the crucial role of a thin graphene platelet layer in diminishing friction and wear. Besides, graphene has demonstrated great potential as a coating material for a variety of surfaces. Recent studies have shown that graphene nanosheets (GNS) can be fully attached to surface peaks and valleys, making them well-suited for use in MDD [19–21]. Research by Nguyen et al. [22] studied an uncomplicated approach employing an ethanol dispersion of few-layer GNS, leveraging the simplicity of air-drying this dispersion. Further efforts to enhance the performance of graphene lubricants involve its synergy with other materials to maximise its intrinsic benefits. Zhao and Ci [23], along with Patel and Kiani [24], both explored the synergistic effect of GNS and TiO<sub>2</sub> NPs in enhancing lubrication properties. Specifically, they found that applying GNS to the exterior of TiO<sub>2</sub> NPs effectively prevents particle agglomeration, leading to an improvement in the wear resistance and friction reduction properties of the TiO<sub>2</sub> nanolubricant. Therefore, it is possible to combine graphene lubricant and TiO<sub>2</sub> nanolubricant as a novel lubricant in the MDD.

This research explores the influence of graphene lubricant and TiO<sub>2</sub> nanolubricant on the forming force and contour precision of microcups during the MDD, utilising SUS301. Four distinct lubrication conditions were scrutinised, comprising dry, 2.0 wt% TiO<sub>2</sub> nanolubricant, 10 mg/ml graphene lubricant, and a combination of 2.0 wt% TiO<sub>2</sub> nanolubricant and 10 mg/ml graphene lubricant. The primary objective is to reduce both the forming force and cup wrinkling, thus enhancing the final product quality. Through this, the study not only contributes towards fine-tuning the MDD process but also provides meaningful perspective on crafting superior-quality microcups.

## 2 Material and experiments

The research made use of SUS301 foils with dimensions of 4.0 mm × 4.0 mm (length × width) and a thickness of 40.0 ± 2.0 μm. Stainless steel was selected as the substrate material for this study due to its widespread utilisation in micro-manufacturing contexts and extensively documented formability characteristics [25]. The detailed chemical compositions of the foil can be found in Table 1.

These foils underwent annealing in an argon-filled KTL tube furnace at 980 °C for a duration of 2.0 min to enhance their crystallinity [26, 27]. The foils were heated in a furnace at a temperature rise of 10 °C/min from room temperature to the target annealing temperature. After holding at the target temperature for 2 min, the foils were cooled to room temperature in the furnace. As demonstrated in Fig. 1, the MDD

**Table 1** Chemical compositions of SUS301 (wt%)

C	Si	Cr	Mn	Ni	N	P	S	Fe
0.15	0.75	16.00–18.00	2.00	6.00–8.00	0.10	0.045	0.030	Balance

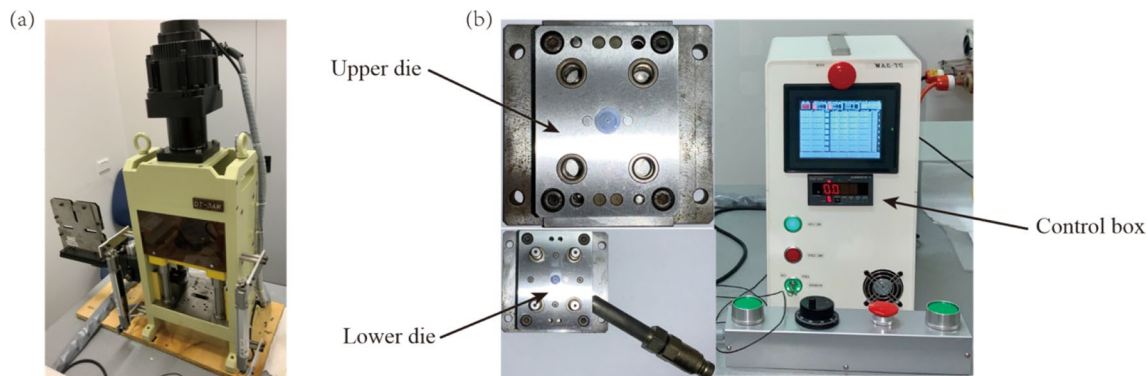


**Fig. 1** Core components of the MDD system. **a** The DT-3AW press machine. **b** Die set and control box

apparatus is structured around three principal components: the DT-3AW press machine, a die set, and a control box. During the MDD experiments, the upper and lower dies were implemented, operating at a drawing speed of 0.1 mm/s. Figure 2 shows the components and dimensions of the die set used in MDD. The upper die contains a micro punch, while the lower die features a cavity. Approximately 0.1 ml of the nanolubricant was dipped into the die cavity in preparation for the MDD studies. The investigation employed a glycerol-based lubricant infused with 2.0 wt% TiO<sub>2</sub> NPs. The lubricant's formulation involved incorporating a designated amount of pure TiO<sub>2</sub> NPs (P25), approximately 20.0 nm in diameter, into distilled water, ensuring a balanced distribution. The mixture was subjected to mechanical stirring and was subsequently treated with polyethyleneimine (PEI), at a concentration of 0.4 wt%, which acted as a dispersant. The mix was then subjected to centrifugation at a rate of 2000 revolutions per minute for a span of 10.0 min, culminating in a stable suspension. The next step involved the dropwise addition of 80 wt% glycerol to the suspension, followed by mechanical stirring at 1800 r/min for 15.0 min and ultrasonication for 15.0 min to promote comprehensive dispersion of the TiO<sub>2</sub> NPs. The final product was a 50.0-g lubricant with a composition of 2.0 wt% TiO<sub>2</sub>, 0.4 wt% PEI, 80.0 wt% glycerol, and a remaining proportion of distilled water. The lubricants underwent ultrasonic treatment for a duration of 20.0 min prior to their utilisation in the MDD tests.

For the integration of the graphene lubricant into the MDD, a dip-coating technique was adopted, employing an ethanol-based graphene lubricant on the test specimens. The process began by blending graphene powder with undiluted ethanol, followed by a 10.0-min mechanical stirring, yielding a graphene lubricant concentration of 10.0 mg/ml. Prior to application, the lubricants were subjected to ultrasonication at 24 °C for 25.0 min. In order to apply GNS onto the

steel foil, a quantity nearing 0.5 ml of the graphene-ethanol blend was carefully dispensed onto the specimen's surface with the aid of a syringe. Once the solvent had evaporated, a thin film of GNS was mechanically coated onto the substrate. Following this, a specimen layered with GNS was positioned on the lower die, after which the MDD commenced using graphene lubricant.

The MDD tests were conducted under four lubrication conditions: dry, TiO<sub>2</sub> nanolubricant, graphene lubricant, and a combination of TiO<sub>2</sub> nanolubricant and graphene lubricant. Each condition was tested five times, with drawing forces measured using a force sensor in the upper die. The shape and surface texture of the resultant microcups were examined using a 3D laser microscope. Energy dispersive spectroscopy (EDS) and scanning electron microscopy (SEM) were employed to examine the remaining traces of titanium and carbon present on the microcups.

## 3 Results and discussion

### 3.1 Characterisation of TiO<sub>2</sub> nanolubricant and graphene lubricants

The analysis of this study crucially centres on the sedimentation behaviour of 2 wt% TiO<sub>2</sub> nanolubricant and 10 mg/ml graphene lubricant. Figure 3 presents the sedimentation behaviour of the lubricants across varying time intervals. The data highlights the impressive stability of the TiO<sub>2</sub> nanolubricant. After a 40-h duration, the TiO<sub>2</sub> NPs maintain their largely undisturbed state, signifying the exceptional dispersion stability of glycerol-based nanolubricants. This superior stability is a desirable property for lubricants, as it can contribute to prolonged operational efficiency. However, the behaviour of the graphene lubricant was different.

**Fig. 2** MDD die set components and geometric dimensions

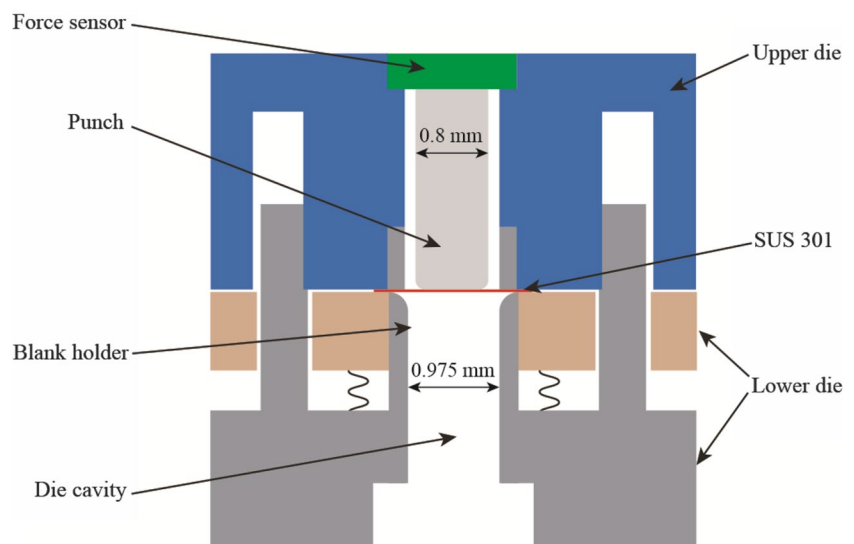
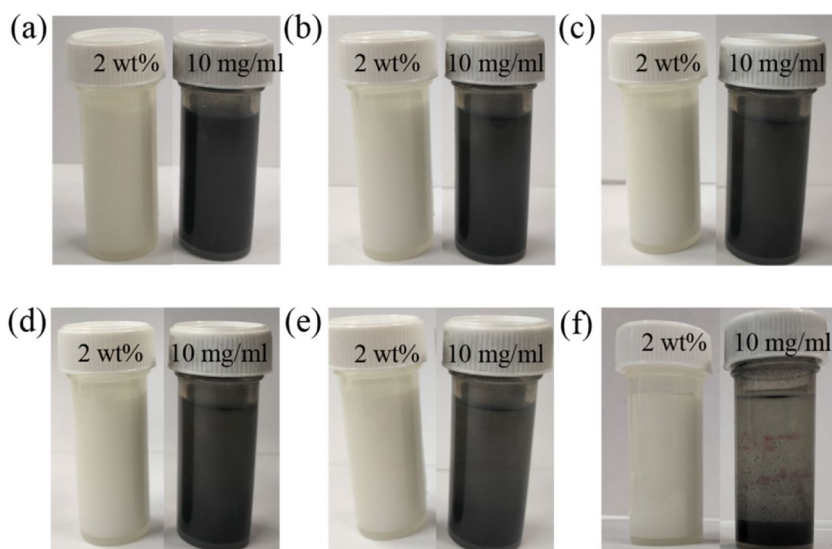


**Fig. 3** Time-dependent sedimentation behaviour of the 2 wt% TiO<sub>2</sub> nanolubricant and 10 mg/ml graphene lubricant. **a** Initial state. **b** 8 h. **c** 16 h. **d** 24 h. **e** 32 h. **f** 40 h

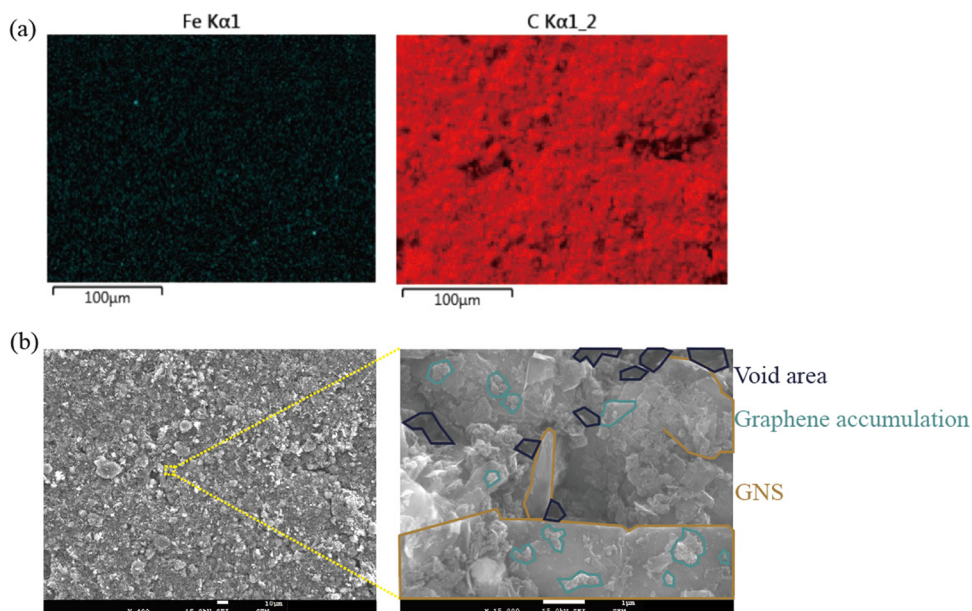


As time progressed, the sedimentation of graphene became increasingly apparent. It was found that significant precipitation of graphene was observed after a relatively short duration of 18 h. Furthermore, after the 40-h duration, the graphene lubricant displayed a state of total sedimentation, indicating that all the graphene had precipitated out of the solution. This behaviour suggests that, compared to the TiO<sub>2</sub> nanolubricant, the graphene lubricant may exhibit a shorter effective lifespan, potentially requiring more frequent monitoring and replacement.

GNS were deposited on the substrate surface through application of the graphene lubricant. Figure 4 displays the EDS maps and SEM images of a tested sample treated with the graphene lubricant. One of the key findings from the EDS maps is the confirmation of the successful application

of graphene onto the sample surface. This is highlighted by the marked distribution of C across the surface, which is a primary constituent of graphene. Complementing, this is the observed distribution of Fe, corroborating the presence and successful adhesion of the graphene lubricant onto the surface. Further enhancing the understanding of the graphene coating is the high-resolution SEM imaging. Through this magnified perspective, the presence of GNS becomes evident. Within the coated region, these GNS predominantly form layered configurations; however, uncoated sections are present. These voids have the potential to diminish the lubrication efficiency of the coating, leading to inadequate performance compared to a consistently coated surface. Graphene powder showed a marked accumulation on the coated GNS, possibly from the convergence of nanosheet clusters.

**Fig. 4** Graphene lubricant coating. **a** EDS mapping. **b** SEM analysis



The graphene accumulation could influence the lubrication efficiency in the synthesis of graphene lubricant and TiO<sub>2</sub> nanolubricants, as it may hinder TiO<sub>2</sub> NPs sliding.

### 3.2 Effect of TiO<sub>2</sub> nanolubricant and graphene lubricant on deep drawing force

During the MDD, the drawing force was recorded. Figure 5 presents the influence of four distinct lubrication conditions on this force. The force–displacement curves in Fig. 5(a) demonstrate a marked increase in drawing force as the process progresses. This pronounced escalation is a consequence of the material experiencing significant deformation. Such plastic deformation heightens the friction at the material-tool interface owing to the considerable contact area and squeeze force. Consequently, lubricant efficacy could be evaluated via quantitative analysis of peak drawing forces under these lubrication conditions. Figure 5 (b) reveals that in dry conditions, the peak drawing force reached 77.56 N. With the use of TiO<sub>2</sub> nanolubricant, the peak drawing force drops to 72.88 N, and under the influence of graphene lubricant, it further diminishes to 66.3 N. The minimum of peak drawing force, at 65.62 N, was achieved when both TiO<sub>2</sub> nanolubricant and graphene lubricant were simultaneously applied. Compared to the dry condition, the combination of TiO<sub>2</sub> nanolubricant and graphene lubricant facilitated a 15.39% reduction in the peak drawing force. On the other hand, the use of TiO<sub>2</sub> nanolubricant and graphene lubricant resulted in a reduction by 6.03% and 14.52%, respectively. The peak drawing force shows 0.87% variation between the 10 mg/ml graphene lubricant and the combined TiO<sub>2</sub> nanolubricant with graphene lubricant. The forming process undergoes two critical transitions beyond the displacement at peak drawing force.

Firstly, the contact area between the workpiece and die cavity expands significantly as forming approaches completion. This marked growth transforms friction into a principal factor governing the process. However, in the displacement range beyond peak drawing force up to 0.93 mm, the drawing force is notably diminished with the synergistic TiO<sub>2</sub> nanolubricant and graphene lubricant compared to sole graphene lubricant or TiO<sub>2</sub> nanolubricant. While the peak drawing forces are comparable with 10 mg/ml graphene lubricant alone and combined TiO<sub>2</sub> nanolubricant + 10 mg/ml graphene lubricant, the drawing force decreases more after peaking when both lubricants are used together. This suggests further that friction reduction is achieved when the GNS spread and mix with the TiO<sub>2</sub> NPs during the drawing process. Following a displacement of 0.93 mm, the drawing force exhibits a notable escalation when employing the synergistic combination of TiO<sub>2</sub> nanolubricant and graphene lubricant, followed by a subsequent decline towards completion. At 0.93 mm displacement, as the forming process nears completion, the combined TiO<sub>2</sub> nanolubricant and graphene lubricant form a prominent boundary film between the material and die cavity. This boundary film withstands the rising blank pressure against the die cavity and intensified punch contact. Consequently, the drawing force exhibits a sharp increase at this advanced stage.

### 3.3 Lubricant effects on wrinkling

The assessment of TiO<sub>2</sub> nanolubricant and graphene lubricant performance highlights their potential in reducing friction during MDD. Notably, these lubricants substantially affect the initiation of wrinkling across the diverse

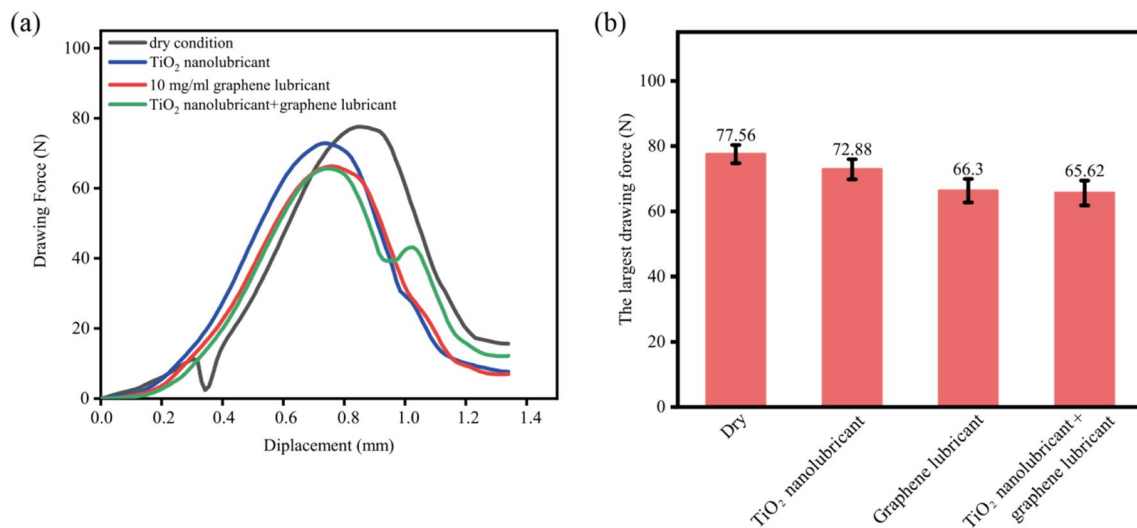


**Fig. 5** **a** Evaluation of drawing force and **b** comparative analysis of peak forces under varied lubrication circumstances

microcups. Microcup wrinkling was quantified using the measurement geometry depicted in Fig. 6. The position coordinates, reference circle, and tensile line were selected accordingly. The wrinkling angle, peak height, and valley height served to determine the wrinkling value through Eqs. 1 and 2:

$$R_{ai} = \frac{R_{vi} + R_{pi}}{2} \quad (1)$$

$$R_w = \sum_{i=1}^N R_{ai} \times \theta_i \quad (2)$$

where,  $R_{ai}$ ,  $R_{pi}$ , and  $R_{vi}$  are the local wrinkle value, peak, and valley at point  $i$ .  $\theta_i$  is the wrinkle angle at point  $i$ .  $R_w$  is the overall wrinkle value for the cup.

The wrinkling is related to energy use at the blank edge. In this region, the primary deformation often manifests as

circumferential compression, while the secondary deformation involves a variety of processes including bending and the thickness direction blank holding. More severe wrinkling might be observed when the energy expended in primary deformation outweighs that of the secondary deformation. Figure 7 (a) shows microcups, viewed from the mouth, produced under diverse lubrication conditions. The samples drawn with lubricants exhibit fewer wrinkles compared to those produced under dry conditions. In particular, the microcup drawn using the TiO<sub>2</sub> nanolubricant displays the least amount of wrinkling. Figure 7 (b) shows the wrinkling value of microcups drawn under dry, TiO<sub>2</sub> nanolubricant, graphene lubricant, and TiO<sub>2</sub> + graphene lubricant respectively. The wrinkling values in Fig. 7(b) indicate significant wrinkling reduction from the lubricants. Under dry conditions, wrinkling value peaks at 125.52  $\mu\text{m}$ . The application of graphene lubricant mitigates this to 81.56  $\mu\text{m}$ , while the TiO<sub>2</sub> nanolubricant further moderates the wrinkling value

**Fig. 6** Wrinkling measurement of drawn cup

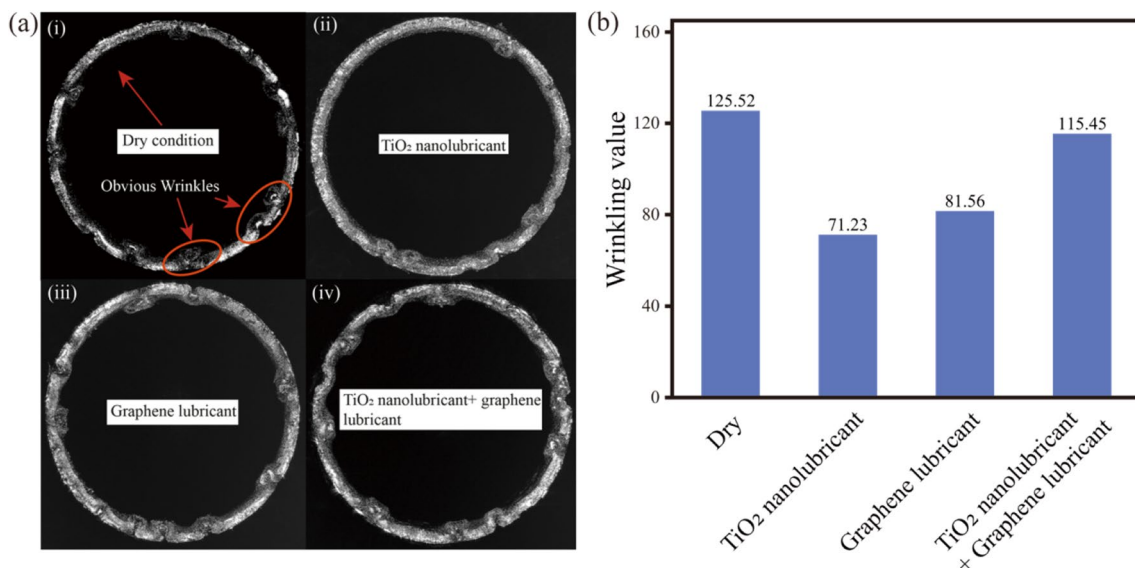
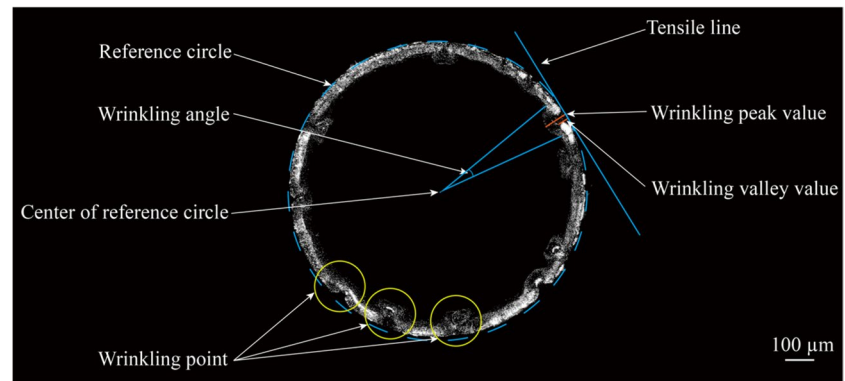


**Fig. 7** **a** View of the mouth of drawn cups from diverse lubrication conditions: (i) dry; (ii) TiO<sub>2</sub> nanolubricant; (iii) graphene lubricant; and (iv) TiO<sub>2</sub> nanolubricant + graphene lubricant. **b** Wrinkling values of drawn cups under varied lubrication conditions

to 71.23  $\mu\text{m}$ . The combined application of  $\text{TiO}_2$  nanolubricant and graphene lubricant results in a wrinkling value of 115.45  $\mu\text{m}$ . Variations in the wrinkling values could be attributed to the performance of the applied lubricants. By reducing friction, the lubricant facilitates smooth blank flow into the die cavity. Reducing the contact time between the blank and blank holder can limit the energy consumed in compression, thus potentially reducing the wrinkling. However, wrinkling is more pronounced with the combined  $\text{TiO}_2$  nanolubricant and graphene lubricant versus either lubricant alone. Though the synergistic effect of the  $\text{TiO}_2$  nanolubricant and graphene lubricant maximises friction reduction, their concurrent use can induce uneven film development at the blank edge. This nonuniform interfacial layer results in inconsistent deformation along the edge, potentially contributing to the aggravated wrinkling.

### 3.4 Lubricant interactions in MDD

Figure 8 presents SEM and EDS analyses illustrating the morphology and elemental composition of microcup surfaces formed with  $\text{TiO}_2$  nanolubrication. This figure exhibits titanium presence concentrated at the edges and lower sections of the microcups. At the initiation of MDD, the edge of the blank undergoes a bending process and experiences substantial pressure from the blank holder [28]. Based on the open lubricant pockets (OLPs) and close lubricant pocket (CLPs) theory, OLPs are situated at the surface edge,

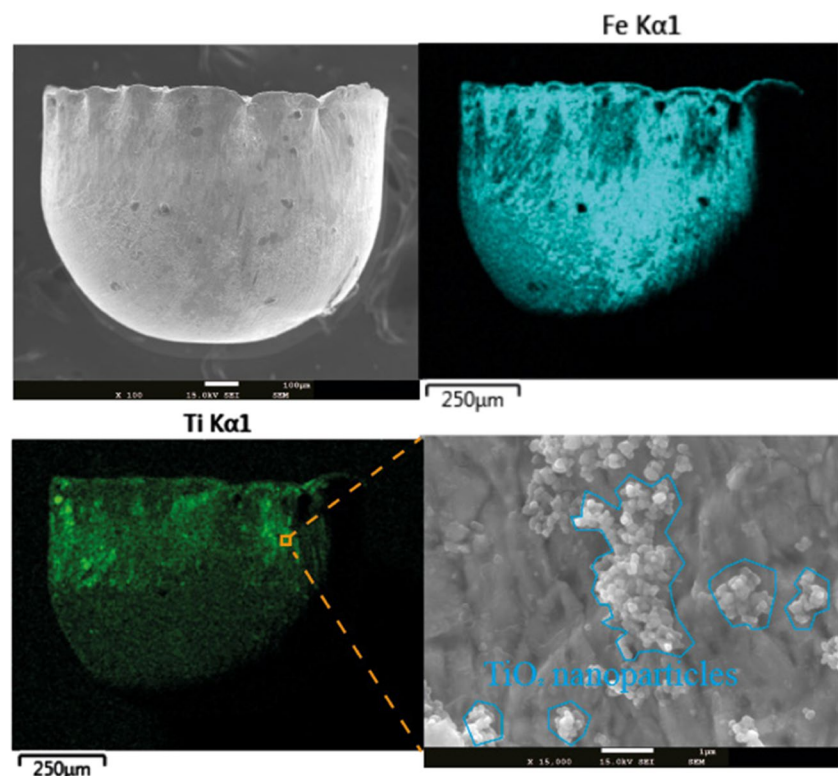
enabling lubricant leakage. CLPs effectively conserve lubricant, reducing the pressure from the applied load. As the forming process causes surface flattening, it expands the actual contact area. The lubricant from the original contact surface and CLPs then relocates, forming a new lubrication film. Figure 9 presents a detailed illustration of the lubrication mechanism employed by  $\text{TiO}_2$  nanolubricant in the MDD. A commonly used theoretical approach for determining the thickness of a lubricating film in hydrodynamic lubrication conditions is based on the Reynolds equation.

$$\frac{\partial}{\partial x} \left( \phi_x \frac{\rho h^3}{12\mu} \frac{\partial p_h}{\partial x} \right) = u \frac{\partial(\rho h_T)}{\partial x} \quad (3)$$

where  $h$  is the film thickness,  $\mu$  is the fluid viscosity,  $\rho$  is the fluid density, and  $u$  is the forming speed.  $\phi_x$  is the pressure flow factor in  $x$  direction and  $h_T$  is the average gap between two surfaces.

This formula reveals an inverse relationship between increasing pressure in the lubricated area and the corresponding film thickness. As the punch moves, it substantially increases the drawing force, which further reduces the thickness of the nanolubricant film. This reduction potentially leads to an insufficient lubricating film. Moreover, the  $\text{TiO}_2$  NPs embedded within the lubricant layer display a behaviour similar to that of ball bearings. By converting sliding movements between contact pairs into rotational movement, they further contribute to the

**Fig. 8** SEM and EDS analysis of microcup surface with 2 wt%  $\text{TiO}_2$  nanolubricant



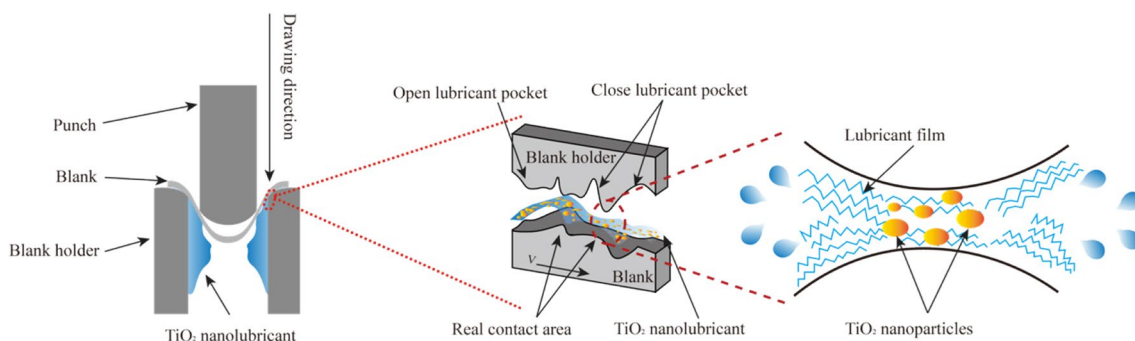


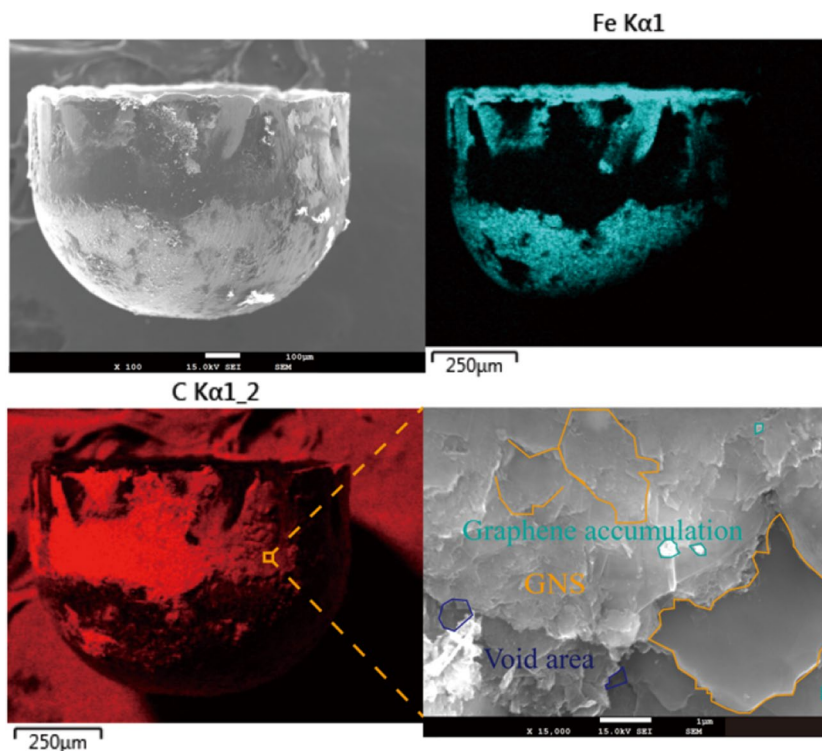
**Fig. 9** The lubrication mechanisms of  $\text{TiO}_2$  nanolubricant in MDD

mitigation of frictional forces during the process. Another notable capability of the  $\text{TiO}_2$  NPs is their ability to fill the surface imperfections and smooth out irregularities. By doing so, they enhance the overall performance of the lubricants, providing a more even and manageable interaction surface for the drawing process. While  $\text{TiO}_2$  nanoparticles offer distinct advantages in lubrication, their tendency towards agglomeration is evident in the SEM analysis. Agglomeration involves nanoparticles clustering into larger groupings due to attractive forces like van der Waals interactions [29]. Within the diffusion environment created by the nanolubricant, NPs initially form loose, branched agglomerates. Shearing can break these apart, but sustained stresses compact the clusters into denser aggregates. Areas of high stress concentration around

defects and dislocations provide optimal conditions for accelerated agglomeration. Detailed image quantification from the SEM data discerns pronounced nanoparticle clusters spread across the surface of the microcup drawn using the  $\text{TiO}_2$  nanolubricant. The clustering changes the effective particle size distribution and reduces the total surface area for lubricant spreading and adhesion. This can deteriorate the friction-reduction and anti-wear properties.

In MDD with  $\text{TiO}_2$  nanolubricant, nanoparticle agglomeration occurs. A potential solution to this challenge is the incorporation of GNS as a solid lubricant [30]. To gain deeper insights into the role of GNS as lubricants in MDD, SEM images and EDS maps of the microcup surfaces were analysed, the results of which are presented in Fig. 10

**Fig. 10** SEM and EDS analysis of microcup surface with 10 mg/ml graphene lubricant





[31]. A salient finding from this analysis is the distributed presence of C element on the microcup, which suggests a residual existence of GNS. EDS image reveals a homogeneous graphene nanosheet film covering over 70% of the formed microcup surface. Correlating this extensive coverage to reduced friction confirms the lubricating mechanism of transferred graphene coatings in MDD. High-resolution scanning electron microscopy discloses the multilayer graphene structure persisting on the microcup surface. This interfacial graphene film acts as a sliding interface, mitigating friction during MDD. Additionally, the SEM analysis discloses reduced graphite accumulation on the microcup surface following graphene-lubricated MDD. This decrease in graphite accumulation is attributed to the relative sliding of GNS between the workpiece and tool, enabled by the lubricating action. Figure 11 shows the operational mechanism of the graphene lubricant in the MDD. This sliding motion of GNS potentially allows the accumulating graphite to fill existing voids on the surface, thereby creating a more uniform and smooth interaction interface. This filling action not only helps in smoothing out the surface but also contributes to a consequent decrease in the friction coefficient. The excellent lubricating performance of graphene lubricant in MDD is attributed to the weak interlayer adhesion and low friction between GNS. The adhesive energy per unit area ( $W$ ) between these graphene layers can be effectively approximated through a formula that specifically applies to weakly interacting layered materials, as follows:

$$W = -\left(\frac{A}{12\pi d^2}\right) \quad (4)$$

where  $A$  is the Hamaker constant ( $\sim 6.5 \times 10^{-20}$  J for graphene),  $d$  is the equilibrium separation distance between the graphene layers ( $\sim 0.34$  nm for graphene).

From this formular, graphene layers exhibit weak adhesion to each other, which allows the layers to slide over one another easily, reducing the friction and wear.

Building on the unique advantages of  $\text{TiO}_2$  nanolubricant and graphene lubricant when used separately, investigating their synergistic effects could be beneficial. As depicted in Fig. 5, the combination of  $\text{TiO}_2$  nanolubricant and graphene lubricant induces a more friction reduction compared to their individual utilisation. Figure 12 displays SEM images and EDS maps of a microcup produced with the combined lubrication of  $\text{TiO}_2$  nanolubricant and graphene lubricant. The synergistic effect of the lubricants enables uniform dispersion of the  $\text{TiO}_2$  NPs. Such improved distribution potentially enhanced the lubrication performance, in addition, the substantial reduction in the agglomeration of  $\text{TiO}_2$  NPs. Figure 13 displays the simultaneous operation of graphene lubricant and  $\text{TiO}_2$  nanolubricants in the MDD. The coating GNS prevent  $\text{TiO}_2$  clusters by providing high surface area for individual NP attachment over clumping. The graphene-NP interaction hinders inter-NP attraction and clustering. These reduced agglomerations suggest a potential for improved lubricating performance when  $\text{TiO}_2$  nanolubricant and graphene lubricants are used concurrently, relative to their individual utilisation. Nonetheless, the observed wrinkling value indicates a potential drawback to this combined method. The dispersion of GNS and  $\text{TiO}_2$  NPs on the blank rim appears uneven. When a lubricating film that merges  $\text{TiO}_2$  NPs and GNS is used, this unevenness at the forming edge may become more pronounced. While the simultaneous use of  $\text{TiO}_2$  nanolubricant and graphene lubricant enhances overall performance compared to their separate application, it also introduces a challenge of less consistent distribution of GNS and  $\text{TiO}_2$  NPs on the blank rim. As the rim undergoes compression and bending from the outset of MDD, using the combined lubricants increases the lubricant amount, which tends to be retained in this region compared to the individual lubricants. This reduced homogeneity impacts the ability of the lubricants to effectively mitigate wrinkling.

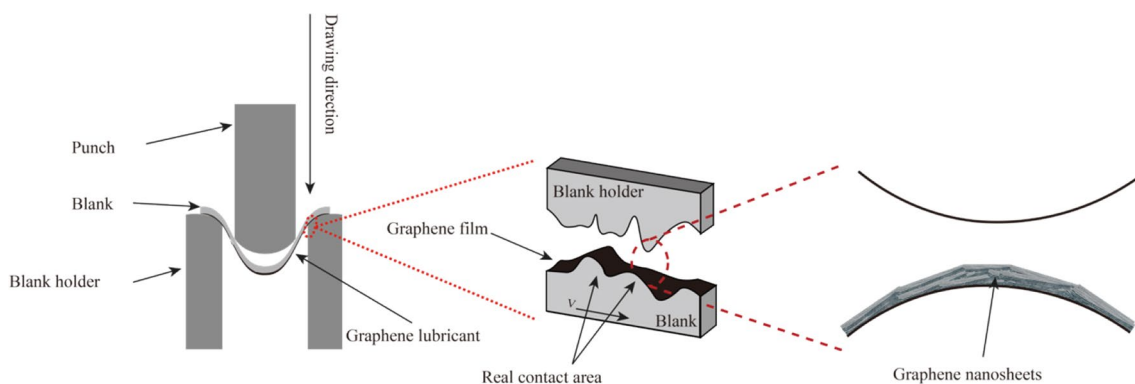
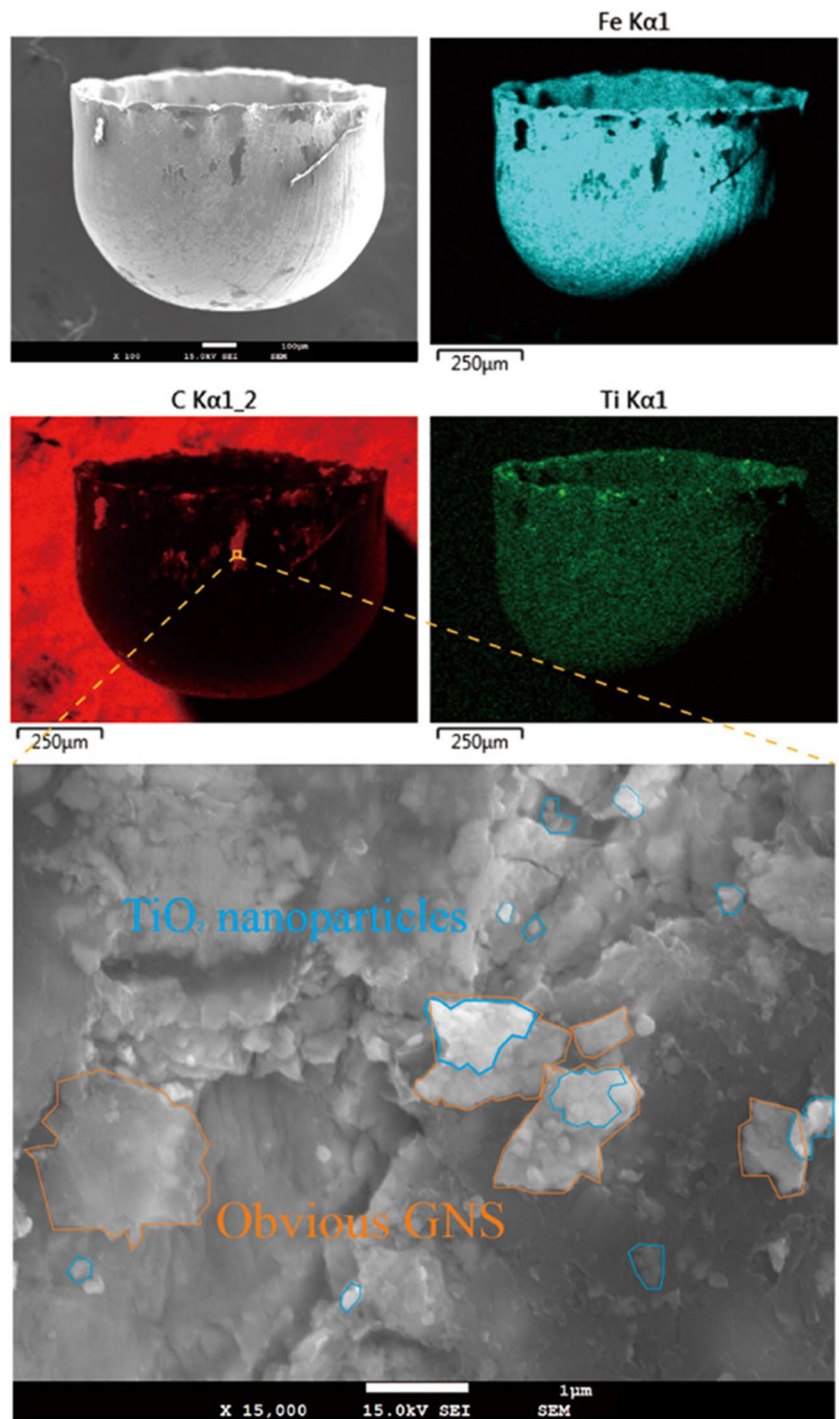


**Fig. 11** Schematic illustrating the mechanism of GNS action in MDD

**Fig. 12** SEM and EDS analysis of microcup surface with 2 wt% TiO<sub>2</sub> nanolubricant + 10 mg/ml graphene lubricant



#### 4 Conclusion

This study shows a considerable reduction in peak drawing force during MDD when utilising lubricants, compared to dry conditions. A synergistic blend of TiO<sub>2</sub> nanolubricant and graphene lubricant delivered the most pronounced reduction in force, slashing it by 15.2% relative to non-lubricated scenarios. Notably, microcups fabricated in the

presence of lubricants exhibited diminished wrinkling, with those drawn using TiO<sub>2</sub> nanolubricant standing out for their minimal wrinkling. SEM images and EDS mappings revealed the persistent adherence of the lubricants to the surface of the micro cup. Introducing TiO<sub>2</sub> nanolubricant to GNS promotes a more homogenous distribution of TiO<sub>2</sub> NPs, significantly reducing their propensity for agglomeration. However, a combined lubricant approach slightly

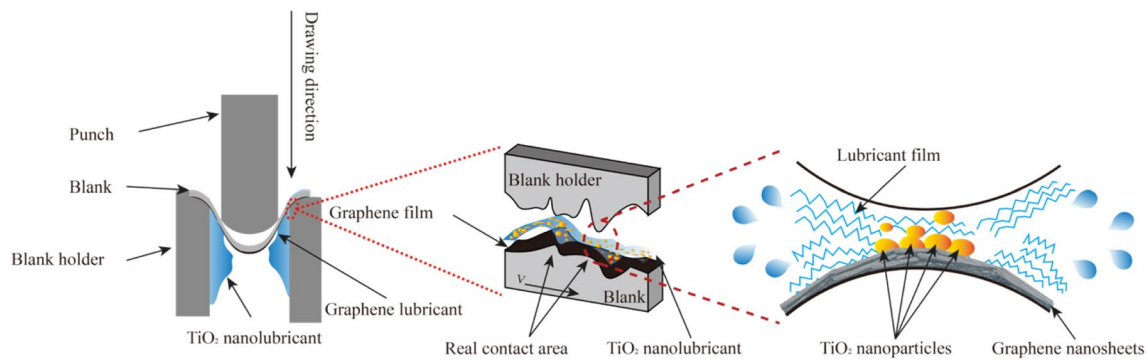


**Fig. 13** The lubrication mechanisms of  $\text{TiO}_2$  nanolubricant and graphene lubricant in MDD

compromises the evenness of GNS and  $\text{TiO}_2$  NP distribution along the rim, leading to a subtle decline in wrinkle mitigation versus their solo applications. In summary, the simultaneous use of these lubricants may not be optimal for achieving the most uniform distribution of GNS and  $\text{TiO}_2$  NPs, but it can still improve the overall performance.

**Funding** Open Access funding enabled and organized by CAUL and its Member Institutions. This research received funding from the Australian Research Council (ARC) through the project designated as DP190100738.

**Data availability** The data sets produced and/or examined during this study can be obtained from the corresponding author upon a reasonable request.

**Code availability** Not applicable.

## Declarations

**Ethics approval** Not applicable.

**Consent to participate** Not applicable.

**Consent for publication** Not applicable.

**Conflict of interest** The authors declare no competing interests.

**Open Access** This article is licensed under a Creative Commons Attribution 4.0 International License, which permits use, sharing, adaptation, distribution and reproduction in any medium or format, as long as you give appropriate credit to the original author(s) and the source, provide a link to the Creative Commons licence, and indicate if changes were made. The images or other third party material in this article are included in the article's Creative Commons licence, unless indicated otherwise in a credit line to the material. If material is not included in the article's Creative Commons licence and your intended use is not permitted by statutory regulation or exceeds the permitted use, you will need to obtain permission directly from the copyright holder. To view a copy of this licence, visit <http://creativecommons.org/licenses/by/4.0/>.

## References

- Jiang Z, Zhao J, Xie H (2017) Microforming technology: theory, simulation and practice. Academic Press
- Irthia I, Green G, Hashim S, Kriama A (2014) Experimental and numerical investigation on micro deep drawing process of stainless steel 304 foil using flexible tools. *Int J Mach Tools Manuf* 76:21–33
- Si S et al (2022) Numerical simulation and experiment of microstamping process to fabricate multi-channel of SUS304 thin sheets with different grain size. *Int J Adv Manuf Technol* 121(9–10):6739–6750
- Luo L, Jiang Z, Wei D (2017) Influences of micro-friction on surface finish in micro deep drawing of SUS304 cups. *Wear* 374:36–45
- Fejkiel R, Goleń P (2023) Application of the finite element method to simulate the friction phenomenon in a strip drawing test. *Adv Mech Mater Eng* 40(1):39–46
- Kim H, Sung JH, Sivakumar R, Altan T (2007) Evaluation of stamping lubricants using the deep drawing test. *Int J Mach Tools Manuf* 47(14):2120–2132
- Azman NF, Samion S (2019) Dispersion stability and lubrication mechanism of nanolubricants: a review. *Int J Precis Eng Manuf-Green Technol* 6:393–414
- Alves SM, Mello V, Faria E, Camargo A (2016) Nanolubricants developed from tiny CuO nanoparticles. *Tribol Int* 100:263–271
- Jason YJJ, How HG, Teoh YH, Chuah HG (2020) A study on the tribological performance of nanolubricants. *Processes* 8(11):1372
- Mousavi SB, Heris SZ, Estellé P (2020) Experimental comparison between ZnO and MoS<sub>2</sub> nanoparticles as additives on performance of diesel oil-based nano lubricant. *Sci Rep* 10(1):5813
- Xie D, Ouyang Q, He L, Xu W (2023) Effect of TiO<sub>2</sub> nanoparticle lubrication on precision forming. *Int J Adv Manuf Technol* 127:1–14
- Trung T, Cho W-J, Ha C-S (2003) Preparation of TiO<sub>2</sub> nanoparticles in glycerol-containing solutions. *Mater Lett* 57(18):2746–2750
- Esfe MH, Rostamian H (2017) Non-Newtonian power-law behavior of TiO<sub>2</sub>/SAE 50 nano-lubricant: an experimental report and new correlation. *J Mol Liq* 232:219–225
- Kumar M, Afzal A, Ramis M (2017) Investigation of physico-chemical and tribological properties of TiO<sub>2</sub> nano-lubricant

- oil of different concentrations. *Tribologia-Finnish J Tribol* 35(3):6–15
15. Zhang J, Chen Z, Wu H, Zhao J, Jiang Z (2019) Effect of graphene on the tribolayer of aluminum matrix composite during dry sliding wear. *Surf Coat Technol* 358:907–912
  16. Berman D, Erdemir A, Sumant AV (2014) Graphene: a new emerging lubricant. *Mater Today* 17(1):31–42
  17. Zhao J, Gao T, Li Y, He Y, Shi Y (2021) Two-dimensional (2D) graphene nanosheets as advanced lubricant additives: a critical review and prospect. *Mater Today Commun* 29:102755
  18. Lin J, Wang L, Chen G (2011) Modification of graphene platelets and their tribological properties as a lubricant additive. *Tribol Lett* 41:209–215
  19. Liu L et al (2019) Recent advances in friction and lubrication of graphene and other 2D materials: mechanisms and applications. *Friction* 7:199–216
  20. Mi Y et al (2012) A simple and feasible in-situ reduction route for preparation of graphene lubricant films applied to a variety of substrates. *J Mater Chem* 22(16):8036–8042
  21. Liu Y, Yu S, Shi Q, Ge X, Wang W (2022) Graphene-family lubricant additives: recent developments and future perspectives. *Lubricants* 10(9):215
  22. Nguyen D et al (2011) Synthesis of ethanol-soluble few-layer graphene nanosheets for flexible and transparent conducting composite films. *Nanotechnology* 22(29):295606
  23. Zhao W, Ci X (2020) TiO<sub>2</sub> nanoparticle/fluorinated reduced graphene oxide nanosheet composites for lubrication and wear resistance. *ACS Appl Nano Mater* 3(9):8732–8741
  24. Patel J, Kiani A (2019) Tribological capabilities of graphene and titanium dioxide nano additives in solid and liquid base lubricants. *Appl Sci* 9(8):1629
  25. Luo L et al (2017) Effects of hydraulic pressure on wrinkling and earing in micro hydro deep drawing of SUS304 circular cups. *Int J Adv Manuf Technol* 90:189–197
  26. Kong D et al (2018) Heat treatment effect on the microstructure and corrosion behavior of 316L stainless steel fabricated by selective laser melting for proton exchange membrane fuel cells. *Electrochim Acta* 276:293–303
  27. Luo L, Wei D, Zu G, Jiang Z (2021) Influence of blank holder-die gap on micro-deep drawing of SUS304 cups. *Int J Mech Sci* 191:106065
  28. Zhao J et al (2021) Experimental investigation on micro deep drawing of stainless steel foils with different microstructural characteristics. *Chin J Mech Eng* 34:1–11
  29. Jang TS et al (2022) Topography-supported nanoarchitectonics of hybrid scaffold for systematically modulated bone regeneration and remodeling. *Adv Func Mater* 32(51):2206863
  30. Zeng X, Peng Y, Lang H (2017) A novel approach to decrease friction of graphene. *Carbon* 118:233–240
  31. Liu Y, Ge X, Li J (2020) Graphene lubrication. *Appl Mater Today* 20:100662

**Publisher's note** Springer Nature remains neutral with regard to jurisdictional claims in published maps and institutional affiliations.

2024-01-25

# Exploring the use of graphene lubricant and TiO<sub>2</sub> nanolubricants in micro deep drawing of stainless steel SUS301

Pan, Di

Springer

---

Pan D, Zhang G, Jia F, et al., (2024) Exploring the use of graphene lubricant and TiO<sub>2</sub> nanolubricants in micro deep drawing of stainless steel SUS301. *The International Journal of Advanced Manufacturing Technology*, Volume 130, February 2024, pp. 5521-5532

<https://doi.org/10.1007/s00170-023-12920-x>

*Downloaded from Cranfield Library Services E-Repository*